OPEN ACCESS
JOURNAL OF ADVANCED DIELECTRICS
Vol. 11, No. 3 (2021) 2140004 (6 pages)

DOI: 10.1142/S2010135X2140004X

Influence of CuO addition on dielectric and piezoelectric properties of $(Bi_{0.5}Na_{0.5})TiO_3$–$BaTiO_3$ lead-free piezoceramics

M. Difeo*, L. Ramajo and M. Castro
Research Institute of Materials Science and Technology (INTEMA)
UNMdP – CONICET Av. Colón 10850
B7606BWV Mar del Plata, Argentina
*maurodifeo@outlook.com.ar; maurodifeo@fi.mdp.edu.ar

Received 23 February 2021; Revised 28 April 2021; Accepted 4 May 2021; Published 16 June 2021

Doping effects of CuO on the sintering behavior and electrical properties of $0.94(Bi_{0.5}Na_{0.5})TiO_3$–$0.06(BaTiO_3)$–$x$CuO (BNT–BT6–$x$Cu) lead-free piezoceramic obtained by the conventional solid-state reaction method were investigated. Regarding the undoped system, it is already known that it presents the best densification values when it is sintered at 1150 °C, however, the doped system was sintered at 1150 °C, 1100 °C, 1050 °C, 1025 °C, and 975 °C to determine the effect of Cu on the densification process. Therefore, it was obtained that the CuO-doped samples sintered at 1050 °C presented the highest density values and therefore were the ones chosen to perform the characterization tests together with the undoped system. The samples were characterized using X-ray diffraction (XRD), Raman microspectroscopy, and scanning electron microscopy (SEM) analysis, whereas the ferroelectric and dielectric properties were evaluated by means of ferroelectric hysteresis loops and impedance spectroscopy studies. As a result, the addition of CuO allowed an improvement in sinterability and densification, with the subsequent grain growth, and the improvement of the piezoelectric coefficient (d_{33}).

Keywords: Lead-free piezoelectric; piezoelectric properties; solid-state reaction; CuO dopant.

1. Introduction

Piezoelectric materials based on lead zirconate titanate (PZT) are widely used in a large number of electronic devices due to their excellent electrical properties.[1,2] Compositionally, PZT ceramics lie near a morphotropic phase boundary (MPB) separating the tetragonal and rhombohedral phases, at a concentration x = ~0.48 of $PbTiO_3$. It is generally known that MPB compositions display anomalously high dielectric and piezoelectric properties due to the enhanced polarizability, produced by the coupling between tetragonal and rhombohedral phases.[3] However, the European Union (EU) legislation restricts the use of hazardous substances and encouraged a strong effort into the science and technology of lead-free piezoceramics.[4]

Bismuth sodium titanates are one of the most studied lead-free piezoceramic families due to the existence of a polymorphic phase boundary between the orthorhombic and tetragonal phases for the $(Bi_{0.5}Na_{0.5})TiO_3$ (BNT) composition. However, the high coercive field (E_c~73 kV/cm), in addition to the relatively high leakage currents, hinders the complete polarization of these ceramics.[5–8]

Therefore, to solve the main drawbacks presented by the BNT composition, $(Bi_{0.5}Na_{0.5})TiO_3$–$BaTiO_3$ (BNT–BT) solid solutions were studied.[9–11] These ceramics present a polymorphic phase transition where good piezoelectric properties are obtained and, consequently, are considered as promising candidates to replace lead-based piezoelectric materials.

Piezoelectric properties of BNT–BT solid solutions can also be modified by the incorporation of additives for specific applications. These additives produce structural defects (oxygen or cationic vacancies) modifying the dielectric and piezoelectric properties of the solid solution. Moreover, some additives reduce the sintering temperature restricting the elements' volatilization and, consequently, diminishing the processing cost. Indeed, for $K_{0.5}Na_{0.5}NbO_3$-based materials, CuO has been successfully utilized to bring the sintering temperature down to as low as ~950 °C.[12–14] In the case of BNT-based materials with 4-wt.% CuO, it can also be obtained a similar sintering temperature in addition to improvements in relative density and dielectric permittivity going from 81.8% and 195 to 96.7% and 494 values, respectively.[6] Moreover, CuO addition into BNT–BT–KNN solid solutions reduces the sintering temperature, as a sintering additive, and benefits the piezoelectric properties. For the composition with 0.01-mol.% CuO, a high unipolar strain of 0.39% under 5 kV/mm contributes to a large d^*_{33} of 780 pm/V at room temperature, which is competitive with the other BNT-based ceramics.[15] This additive can also be used to improve the low mechanical quality factor, Q_m, from 72 for

*Corresponding author.

the pure KNN to a very high value of 1965 in 1 mol.% CuO-doped ceramic. Remembering that the Q_m factor is a parameter that measures the relationship between the stored energy and the energy dissipated during a complete signal cycle, a high Q factor indicates a low rate of energy loss relative to the energy stored by the resonator.[16] However, beyond the reduction in sintering temperature, the doping with CuO is accompanied by a pronounced impact on defect structure owing to the formation of defect dipoles as well as on the piezoelectric properties.

Taking into account the previous results reported by other researchers, different amounts of CuO (x = 0, 0.5, 1, and 2 mol.%) were added to the $0.94(Bi_{0.5}Na_{0.5})TiO_3$–$0.06BaTiO_3$ polymorphic phase boundary composition synthesized by the solid-state method. The sintering temperature at which the best densities are obtained was determined and finally the structural, microstructural, dielectric, and piezoelectric properties were evaluated.

2. Materials and Methods

2.1. *Sample preparation*

Lead-free ceramics with the composition $0.94(Bi_{0.5}Na_{0.5})$-TiO_3–$0.06(BaTiO_3)$–xCuO (BNT–BT6–xCu, x = mole percentage) were synthesized by the conventional solid-state reaction method. Then, different excess amounts of CuO (0, 0.5, 1, and 2 mol.%) were introduced. For the synthesis, Bi_2O_3 (Sigma Aldrich, 99.9%), TiO_2 (Sigma Aldrich, 99%), Na_2CO_3 (Biopack, 99.5%), $BaCO_3$ (Merck, 99.5%), and CuO (Mallinckrodt, 99,7%) were mechanochemically activated, using zirconia balls in an alcoholic medium for 3 h, in a planetary mill (Fritsch, Pulverisette 7, 1450 rpm) and thermally treated at 850 °C for 2 h. The obtained powders of each composition were uniaxially pressed into disks and sintered at different temperatures (975 °C, 1025 °C, 1050 °C, 1100 °C, and 1150 °C) for 2 h, employing heating and cooling rates of 5 °C/min.

2.2. *Structural and microstructural characterization*

Crystalline phases were characterized by X-ray diffraction (XRD; PANalytical, X'pert Pro, Cu-Kα). Density values were determined using the Archimedes method. Ceramic samples were polished and grain boundaries were highlighted through a thermal etching step employing a heat treatment which consists of keeping the sample at 50 °C below the sintering temperature for 20 min. Etched samples were analyzed by scanning electron microscopy (SEM; Jeol JSM-6460LV). Raman analyses of samples were performed on a multichannel Renishaw in via Reflex microspectrometer. Excitation was provided by the 514-nm line of an Ar laser. Totally 30–50 scans were performed with an exposure time of 15 s and with a laser power between 30 mW and 300 mW to improve the signal-to-noise ratio.

2.3. *Electrical characterization*

In order to perform the electrical measurements, silver electrodes were painted on both plane-parallel sides of the samples and fired at 700 °C for 20 min. An impedance analyzer (Hewlett-Packard, HP4284A) was used to determine the temperature dependence of the dielectric properties (frequency range from 100 Hz to 1 MHz). Samples were polled by applying a DC field of 30 kV/cm for 10 min in a silicone oil bath at 90 °C. The piezoelectric constant d_{33} was measured using a piezo d_{33} meter (YE2730A d_{33} Meter, APC International, Ltd., USA). The polarization–electric field (P–E) hysteresis loops were measured in a modified Sawyer–Tower circuit using a silicon at room temperature.

3. Results and Discussion

3.1. *Materials characterization*

From the XRD patterns of BNT–BT6–xCu samples at room temperature (RT) [Fig. 1(a)], it was confirmed a single-phase perovskite structure without the formation of secondary phases. Figure 1(b) shows the peaks between $39° < 2\theta < 41°$ corresponding to the (003) and (021) planes and the other peaks between $45.5° < 2\theta < 47.5°$ corresponding to the (202) plane of the rhombohedral structure, typical of pure $Bi_{0.5}Na_{0.5}TiO_3$. However, it can be seen a co-existence between tetragonal and rhombohedral symmetries by the splitting of the (202) plane into (002) and (200) planes suggesting the stabilization of an MPB structure.[14,15] Besides, from the obtained patterns, lattice changes with CuO addition were not observed.

Figure 2 shows the relationship between sintering temperature and density (Archimedes method) for BNT–BT6–xCu ceramics sintered at 975 °C, 1025 °C, 1050 °C, 1100 °C, and 1150 °C. In previous reports, it has been determined that undoped BNT–BT6 samples achieve the highest densification value when the sintering temperature is 1150 °C.[9–11] Taking into account these results, undoped samples were sintered at 1150 °C and the determined density was 5.67 g/cm^3. The doped samples sintered at 1050 °C showed a significant increase in the degree of densification for the entire range of the analyzed compositions. In the case of the doped samples sintered at 1025 °C, 1100 °C, and 1150 °C, the values were slightly higher compared to the undoped system. However, the sintering temperature of 975 °C was insufficient to achieve densification, obtaining considerably lower density values. Therefore, it was found that CuO doping was effective for lowering the sintering temperature of BNT–BT6 by 100 °C without the deterioration of densities. In what follows, the characterization analysis will be focused upon BNT–BT6–xCu samples sintered at 1050°C, since they gave the highest density values, and the results will be compared with the undoped system, which sinters optimally at 1150°C.

Figure 3 shows SEM images of polished and thermally etched BNT–BT6–xCu ceramics, which were sintered at

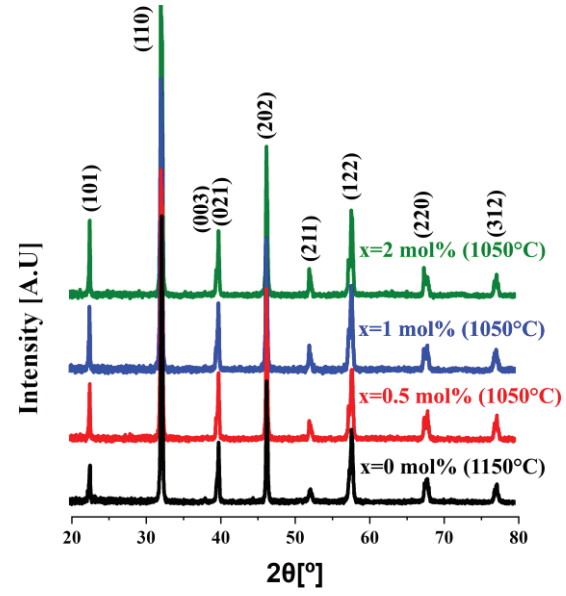

(a)

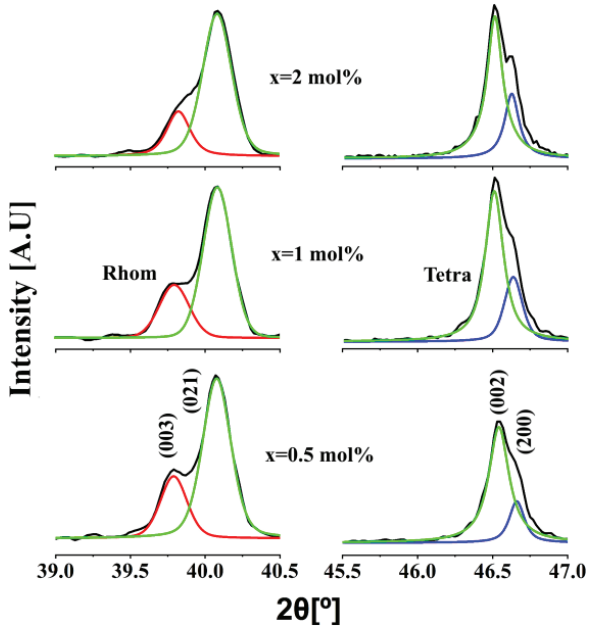

(b)

Fig. 1. (a) XRD patterns of BNT–BT6–*x*Cu sintered ceramics. (b) Details of the XRD patterns in the 39–40.5° and 45.5–47° ranges.

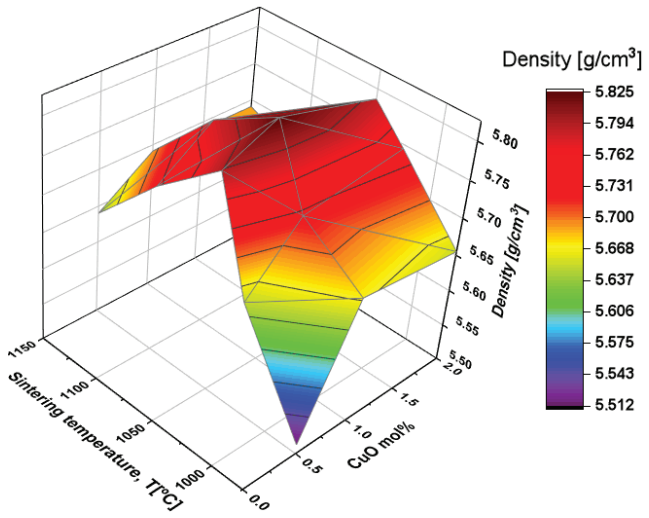

Fig. 2. Density as a function of sintering temperature of BNT–BT6–*x*Cu (*x* = 0.5, 1, and 2 mol.%).

1050 °C, and the undoped BNT–BT6 (sintered at 1150 °C). Sintered ceramics exhibit dense homogeneous microstructures with low porosity, where the pores are located mainly at grain boundaries and triple points. Figure 4 shows the relationship between the medium grain size and the addition amount of CuO. The average grain size of undoped BNT–BT6–*x*Cu (*x* = 0) was close to ~0.82 ± 0.42 μm. The doped samples showed an increment in the mean grain size with the addition of CuO. As in previous reports,[14,15] this behavior was attributed to the formation of a liquid phase by CuO doping along the grain boundaries, which improves sinterability and allows grain growth.

Raman spectroscopy was used to confirm the presence of an MPB because it is highly sensitive to the perovskite distortion.[17] Figure 5 shows the Raman spectra of BNT–BT6–*x*Cu sintered samples, where the results obtained are in agreement with previously reported data.[17,18] As is known, the BNT–BT system presents a co-existence between tetragonal and rhombohedral symmetries,[19] however, CuO addition introduces a distortion in the lattice and therefore changes in the spatial distribution are observed. The mode at 130 cm^{-1} is associated with the Na–O vibration. The broadband composed

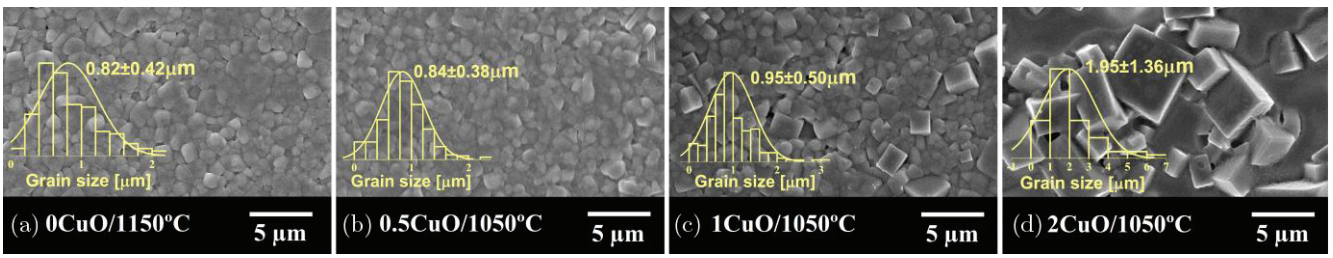

Fig. 3. SEM micrographs and grain size distributions of BNT–BT6–*x*Cu ceramics: (a) *x* = 0 mol.% (1150 °C), (b) *x* = 0.5 mol.% (1050 °C), (c) *x* = 1 mol.% (1050 °C), and (d) *x* = 2 mol.% (1050 °C).

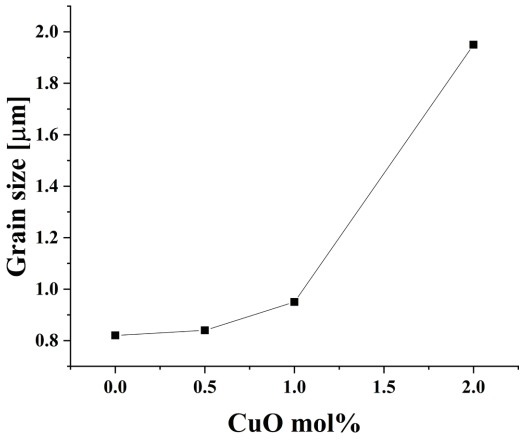

Fig. 4. Evolution of the grain size with the CuO content.

of the peaks 157, 273, 314, and 404 cm^{-1} is dominated by the Ti–O vibration,[20,21] whereas the bands at 533 cm^{-1} and 616 cm^{-1}, approximately, can be assigned to the Ti–O–Ti stretch in edge-shared TiO_6. Bands close to 765 cm^{-1} and 856 cm^{-1} are related to a short Ti–O stretching vibration in distorted TiO_6.[11,22,23] From Fig. 5(a), the co-existence of the

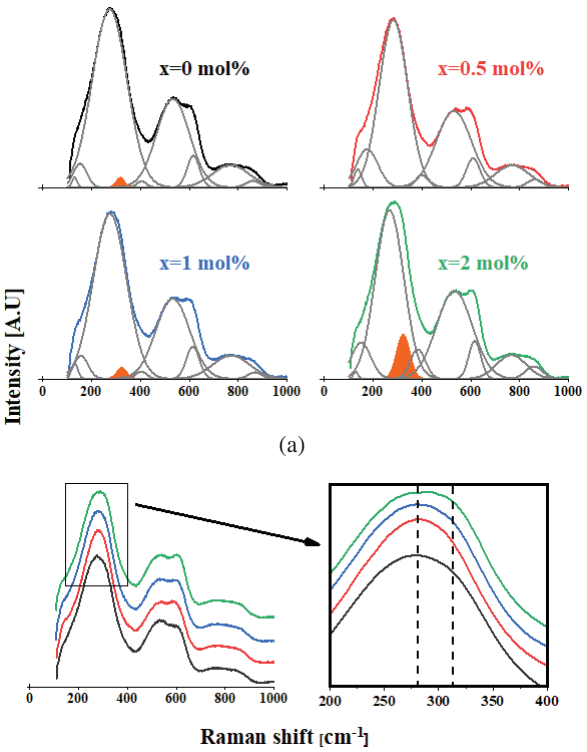

Fig. 5. (Color online) Raman spectra of BNT–BT6–*x*Cu sintered samples: (a) the evolution of the tetragonal phase (orange peak) and (b) the asymmetry of the band 273 cm^{-1} are observed. Black, red, blue, and green lines correspond to $x = 0$, 0.5, 1, and 2 mol.%, respectively.

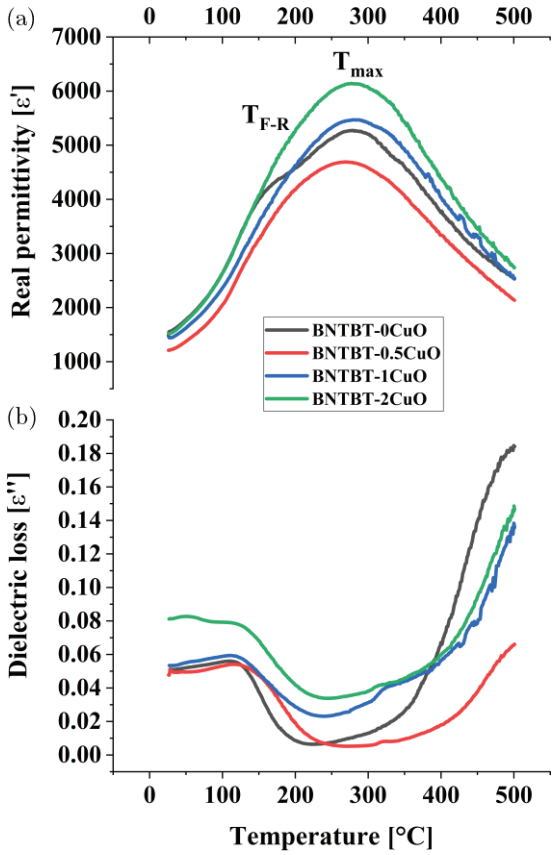

Fig. 6. Temperature dependence of (a) the real permittivity and (b) the dielectric loss (at 1 kHz) of BNT–BT6–*x*Cu ceramic samples.

rhombohedral and tetragonal phases in the undoped system is confirmed by the appearance of a band at ~314 cm^{-1} which corresponds to a tetragonal symmetry.[24] However, the broad-band at 273 cm^{-1} causes difficulty in the visualization of the band at 314 cm^{-1}. Although the shoulder at 314 cm^{-1} is not completely defined, the asymmetry rises as the amount of CuO increases, which reflects the contribution of this peak [see Fig. 5(b)] and therefore the tetragonal phase increases for doping higher than 0.5 mol.%.

Dielectric curves as a function of the temperature of BNT–BT6 sintered at 1150 °C and BNT–BT6–*x*Cu sintered at 1050 °C are shown in Fig. 6. BNT–BT6–*x*Cu samples exhibit high real permittivity values in the analyzed temperature range presenting a ferroelectric–relaxor transition temperature (T_{FR}) in the 140–180 °C region which corresponds to the nonergodic relaxor-to-ergodic relaxor transition that indicates the existence of some relaxing mechanisms at temperatures higher than RT.[25] The wide peak at 300 °C (T_{max}) reveals the existence of a diffuse phase transition (DPT) with high permittivity (ε_r). The dielectric permittivity at T_{max} and RT increases with the concentration of CuO, however, the sample with $x = 0.5$ mol.% presents a curve below the undoped system. Additionally, the dielectric anomaly peaks at T_{max}, for all the ceramics, are relatively broad, where real

dielectric permittivity reached a maximum value of ~6000 ε_0 for BNT–BT6–2Cu samples. The same sequence between the relative amounts of tetragonal phase analyzed by Raman spectroscopy (see Fig. 5) and the variation of the permittivity can be observed. In this way, the sample with $x = 0.5$ mol.% shows a decrease in tetragonality and permittivity regarding undoped samples, which then increase with the dopant content. Furthermore, from Fig. 6(b), it is observed that the first drop of dielectric loss corresponds to the transition temperature T_{FR} and it rises when reaching T_{max}, which is the typical behavior of ceramic relaxors. Comparing the dielectric curves of all samples, variations in the transition temperatures are observed, which suggest that CuO addition affects the dielectric properties of the base system. Nevertheless, due to the detection limit of the XRD equipment, significant changes in the lattice parameters were not observed.

On the other hand, the hysteresis loops at room temperature were influenced by CuO addition. Figure 7 shows the shape of the polarization hysteresis loops of sintered samples, at room temperature. All hysteresis loops have an elliptical shape indicating a lossy dielectric response, and that the saturated polarization was not reached. Although, due to equipment limitations, it is not possible to determine with precision the P_r and E_c values because the applied fields are below the one required to achieve polarization switching, the doped samples produced lower coercive field values than the undoped sample ($E_c = 9.1$ kV/cm). Effectively, for the samples with $x = 0.5$ mol.% and 1 mol.% similar coercive fields were obtained ($E_c = 7.5$ kV/cm), while for the sample with $x = 2$ mol.% it was $E_c = 8.5$ kV/cm. In the case of remnant polarization, the sample doped with $x = 2$ mol.% presented a value, $P_r = 9.4$ mC/cm^2, practically equal to the undoped system, however in the doped ones with $x = 0.5$ mol.% and 1 mol.% the remnant polarization decreased to $P_r = 6.2$ μC/cm^2 and 5.6 μC/cm^2, respectively. Under the applied fields, it can be observed that the hysteresis loops have the contribution of all other polarization mechanisms but for the intrinsic dipoles' reorientation polarization mechanism.

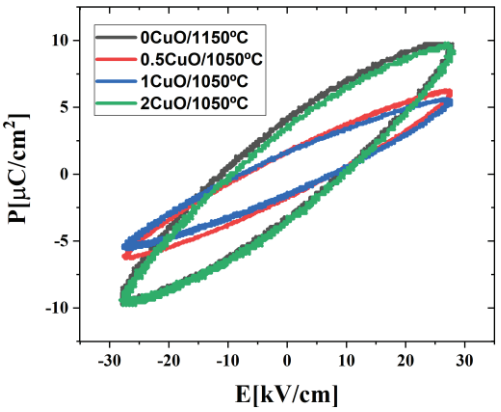

Fig. 7. Hysteresis loops at room temperature of BNT–BT6–xCu ($x = 0$, 0.5, 1, and 2 mol.%).

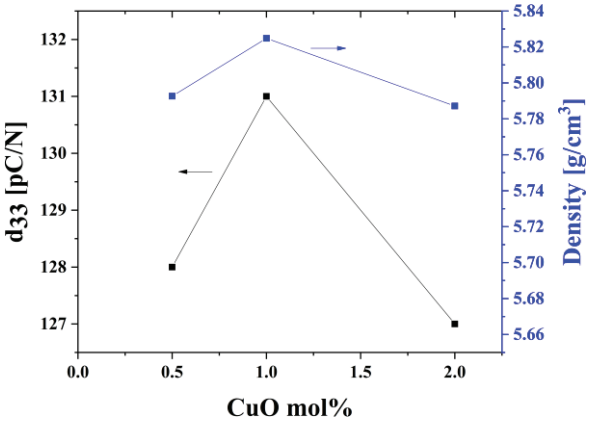

Fig. 8. The d_{33} and density values of BNT–BT6–xCu as a function of CuO amount.

Figure 8 shows the piezoelectric coefficient (d_{33}) as a function of CuO content, and it turned out that d_{33} increased with increasing the CuO amount and showed the maximum value of $d_{33} = 131$ pC/N at $x = 1$ mol.% of CuO which corresponds to the sample with the highest density value, $\rho = 5.83$ g/cm^3.

4. Conclusion

The influence of CuO addition on dielectric and piezoelectric properties of $(Bi_{0.5}Na_{0.5})TiO_3$–$BaTiO_3$-based ceramics was investigated. BNT–BT6–xCu samples were obtained by the solid-state reaction synthesis method and it was observed that the functional properties were strongly dependent on the concentration of the incorporated additive. CuO allowed to improve the sinterability and the density of the system; more precisely, the sintering temperature was reduced from 1150 °C to 1050 °C (by 100 °C) and the density regarding the undoped system increased from 5.67 g/cm^3 to 5.83 g/cm^3 for the composition $x = 1$ mol.%. Moreover, for this composition the highest piezoelectric coefficient (d_{33}) was achieved. Additionally, a small amount of Cu ions could substitute into the lattice site of the perovskite structure, whereas excessive CuO addition was accompanied by a notable grain growth due to the formation of a liquid phase during the sintering process. Dielectric permittivity and loss values showed that the transition temperatures T_{FR} and T_{max} were modified while Raman spectroscopy showed that the relative amount of rhombohedral and tetragonal phases varied with the content of Cu, therefore these changes suggested that Cu ions modified the perovskite structure.

Acknowledgments

The authors would like to thank National University of Mar del Plata (Argentina) Project (15/G577) for providing financial support.

References

[1]C. C. Jin, F. F. Wang, L. L. Wei, J. Tang, Y. Li, Q. R. Yao, C. Y. Tian and W. Z. Shi, Influence of B-site complex-ion substitution on the structure and electrical properties in $Bi_{0.5}Na_{0.5}TiO_3$-based lead-free solid solutions, *J. Alloys Compd*. **585**, 185 (2014).

[2]W. S. Kang and J. H. Koh, $(1-x)Bi_{0.5}Na_{0.5}TiO_3$–$xBaTiO_3$ lead-free piezoelectric ceramics for energy-harvesting applications, *J. Eur. Ceram. Soc.* **35**, 2057 (2015).

[3]T. Shrout and S. Zhang, Lead-free piezoelectric ceramics: Alternatives for PZT?, *J. Electroceramics* **19**, 113 (2007).

[4]European Commission, EU-Directive 2002/95/EC: Restriction of the use of certain hazardous substances in electrical and electronic equipment (RoHS), *Official Journal of the European Union* **46**, 19 (2003).

[5]W.-S. Kang, S.-K. Lee and J.-H. Koh, AC conductivity and dielectric properties of (Bi,Na)TiO_3–$BaTiO_3$ lead-free ceramics, *Ceram. Int.* **41**, 6925 (2015).

[6]R. Dittmer, K. G. Webber, E. Aulbach, W. Jo, X. Tan and J. Rödel, Electric-field-induced polarization and strain in $0.94(Bi_{1/2}Na_{1/2})TiO_3$–0.06 $BaTiO_3$ under uniaxial stress, *Acta Mater*. **61**, 1350 (2013).

[7]M. Cernea, L. Trupina, C. Dragoi, B. S. Vasile and R. Trusca, Structural and piezoelectric characteristics of BNT–$BT_{0.05}$ thin films processed by sol–gel technique, *J. Alloys Compd*. **515**, 166 (2012).

[8]T. Takenaka and K. Sakata, Dielectric, piezoelectric and pyroelectric properties of $(BiNa)_{1/2}TiO_3$-based ceramics, *Ferroelectrics* **95**, 153 (1988).

[9]M.-L. Zhao, C.-L. Wang, J.-F. Wang, H.-C. Chen and W.-L. Zhong, Enhanced piezoelectric properties of $(Bi_{0.5}Na_{0.5})_{1-x}Ba_xTiO_3$ lead-free ceramics by sol-gel method, *Acta Phys. Sin*. **53**, 2357 (2004).

[10]C. Ma, X. Tan, E. Dul'Kin and M. Roth, Domain structure-dielectric property relationship in lead-free $(1-x)(Bi_{1/2}Na_{1/2})$-TiO_3–$xBaTiO_3$ ceramics, *J. Appl. Phys*. **108**, 104105 (2010).

[11]C. Ma and X. Tan, Phase diagram of unpoled lead-free $(1-x)$-$(Bi_{1/2}Na_{1/2})TiO_3$–$xBaTiO_3$ ceramics, *Solid State Commun*. **150**, 1497 (2010).

[12]M. Matsubara, T. Yamaguchi, K. Kikuta and S. Hirano, Sinterability and piezoelectric properties of (K,Na)NbO_3 ceramics with novel sintering aid, *J. Appl. Phys*. **43**, 7159 (2004).

[13]H.-Y. Park, J.-Y. Choi, M.-K. Choi, K.-H. Cho, S. Nahm, H.-G. Lee and H.-W. Kang, Effect of CuO on the sintering temperature and piezoelectric properties of $(Na_{0.5}K_{0.5})NbO_3$ lead-free piezoelectric ceramics, *J. Am. Ceram. Soc.* **91**, 2374 (2008).

[14]W. Jo *et al*., CuO as a sintering additive for $(Bi_{1/2}Na_{1/2})TiO_3$–$BaTiO_3$–$(K_{0.5}Na_{0.5})NbO_3$ lead-free piezoceramics, *J. Eur. Ceram. Soc.* **31**, 2107 (2011).

[15]Z.-H. Zhao, R.-F. Gey and Y. Dai, Large electro-strain signal of the BNT–BT–KNN lead-free piezoelectric ceramics with CuO doping, *J. Adv. Dielect.* **9**, 1950022 (2019).

[16]T. Wang, D. Wang, Y. Liao, Q. Zheng, H. Sun, K. W. Kwok, N. Jiang, W. Jie, C. Xu and D. Lin, Defect structure, ferroelectricity and piezoelectricity in Fe/Mn/Cu-doped $K_{0.5}Na_{0.5}NbO_3$ lead-free piezoelectric ceramics, *J. Eur. Ceram. Soc.* **38**, 4915 (2018).

[17]D. Rout, K.-S. Moon, V. Rao and S.-J. Kang, Study of the morphotropic phase boundary in the lead-free $Na_{1/2}Bi_{1/2}TiO_3$-$BaTiO_3$ system by Raman spectroscopy, *J. Ceram. Soc. Jpn*. **117**, 797 (2009).

[18]B. Wylie-van Eerd, D. Damjanovic, N. Klein, K. Setter and J. Trodahl, Structural complexity of $(Na_{0.5}Bi_{0.5})TiO_3$-$BaTiO_3$ as revealed by Raman spectroscopy, *Phys. Rev. B* **82**, 104112 (2010).

[19]A. Espinosa, J. Camargo, A. del Campo, F. Rubio-Marcos, M. Castro and L. Ramajo, Exploring new methodologies for the identification of the morphotropic phase boundary region in the (BiNa)TiO_3-$BaTiO_3$ lead free piezoceramics: Confocal Raman microscopy, *J. Alloys Compd.* **739**, 799 (2018).

[20]Q. Xu, Z. Song, W. Tang, H. Hao, L. Zhang, M. Appiah, M. Cao, Z. Yao, Z. He and H. Liu, Ultra-wide temperature stable dielectrics based on $Bi_{0.5}Na_{0.5}TiO_3$–$NaNbO_3$ system, *J. Am. Ceram. Soc.* **98**, 3119 (2015).

[21]J. Anthoniappen, C. S. Tu, P.-Y. Chen, C.-S. Chen, Y. U. Idzerda and S.-J. Chiu, Raman spectra and structural stability in B-site manganese doped $(Bi_{0.5}Na_{0.5})_{0.925}Ba_{0.075}TiO_3$ relaxor ferroelectric ceramics, *J. Eur. Ceram. Soc.* **35**, 3495 (2015).

[22]Y. Jia, X. Wei, L. Xu, C. Wang, P. Lian, S. Xue and Y. Shi, Multiphysics vibration FE model of piezoelectric macro fibre composite on carbon fibre composite structures, *Compos. B, Eng*. **161**, 376 (2019).

[23]S. Zhu, L. Cao, Z. Xiong, C. Lu and Z. Gao, Enhanced piezoelectric properties of 3-1 type porous $0.94Bi_{0.5}Na_{0.5}TiO_3$-$0.06BaTiO_3$ ferroelectric ceramics, *J. Eur. Ceram. Soc*. **38**, 2251 (2017).

[24]S. Prasertpalichat, T. Siritanon, N. Nuntawong and D. P. Cann, Structural characterization of A-site nonstoichiometric $(1-x)Bi_{0.5}Na_{0.5}TiO_3$–$xBaTiO_3$ ceramics, *J. Mater. Sci*. **54**, 1162 (2018).

[25]M. Vögler, J. E. Daniels and K. G. Webber, Absence of toughening behavior in $0.94(Na_{0.5}Bi_{0.5})TiO_3$-0.06 $BaTiO_3$ relaxor ceramic, *Scr. Mater.* **136**, 115 (2017).